FULL PAPER

Discovery and Evaluation of a Functional Ternary Polymer Blend for Bone Repair: Translation from a Microarray to a Clinical Model

Ferdous Khan, James O. Smith, Janos M. Kanczler, Rahul. S. Tare, Richard O.C. Oreffo, and Mark Bradley**

Skeletal tissue regeneration is often required following trauma, where substantial bone or cartilage loss may be encountered and is a significant driver for the development of biomaterials with a defined 3D structural network. Solvent blending is a process that avoids complications associated with conventional thermal or mechanical polymer blending or synthesis, opening up large areas of chemical and physical space, while potentially simplifying regulatory pathways towards in vivo application. Here ternary mixtures of natural and synthetic polymers were solvent blended and evaluated as potential bone tissue engineering matrices for osteoregeneration by the assessment of growth and differentiation of STRO-1+ skeletal stem cells. Several of the blend materials were found to be excellent supports for human bone marrow-derived STRO-1+ skeletal cells and fetal skeletal cells, with the optimized blend exhibiting in vivo osteogenic potential, suggesting that these polymer blends could act as suitable matrices for bioengineering of hard tissues.

1. Introduction

Tissue engineering is an interdisciplinary field of research which aims to aid the repair or regeneration of tissue and draws upon the mechanical, biological and chemical properties of materials, cells and a variety of molecules, either alone or in combination.[1–3] Pivotal to this are polymeric biomaterials, which have been utilized in tissue engineering strategies for a variety of potential clinical applications, including the replacement of bone,[4–7] cartilage,[8–10] skin[11–14] and cardiac tissues.[15] Skeletal tissue regeneration is often required following trauma, where substantial bone or cartilage loss may be encountered. In addition, surgically-induced skeletal defects may be produced following debridement of lesions or during revision arthroplasty surgery, where there is a particular unmet need to develop strategies for the replacement of lost bone stock.[16]

For osteoregenerative applications, synthetic scaffolds must be biocompatible, with a highly porous 3D network structure that resembles the natural extracellular matrix, while displaying surface chemistry that promotes cellular attachment, proliferation and differentiation, and enables vascularization and mineral deposition. Furthermore scaffolds need to exhibit sufficient mechanical strength to withstand the stresses of physiological loading to which they will be subjected.[16]

In an ideal scenario, scaffolds should have a 3D porous interconnected network structure, with porosity >60%[17] and individual pores that range from submicron to macro in size,[18,19] which favors the maintenance of cellular activity,[20] nutrient exchange[21] and bone function.[22,23] If a scaffold is to be bioresorbable it must have controlled and highly reproducible resorption profiles, producing non-toxic by-products, whilst maintaining sufficient structural integrity until the newly grown host tissue is able to replace or restore the function of the native tissue.[24] These requirements place extremely challenging demands on the polymer design process.[25]

To address these challenging issues, high-throughput strategies have been developed for the design, synthesis and screening of polymer arrays.[6,26–29] with 3D polymer scaffold libraries fabricated to understand and characterize cell-material interactions and discover useful new materials.[6,30]

The generation of biomedical matrices for tissue regeneration via blending is an attractive approach as it avoids the need to synthesize new polymers,[30–33] offers significant versatility, simplicity and potentially reduces regulatory hurdles while the blended materials can provide either a synergistic combination of physical, biological and chemical properties of the individual polymers,[34,35] or the generation of totally new properties.[6,30]

In this study, polymer microarrays of new polymeric materials were developed via tri-polymer blending (**Figure 1**a) with solution processing to achieve the generation of a porous network structure.[6,30,34] These were analyzed for their ability to

Dr. F. Khan, Prof. M. Bradley
EaStChem, School of Chemistry
University of Edinburgh
Edinburgh, United Kingdom, EH9 3JJ, UK
E-mail: mark.bradley@ed.ac.uk
Dr. J. O. Smith, Dr. J. M. Kanczler, Dr. R. S. Tare, Prof. R. O. C. Oreffo
Bone and Joint Research Group
Human Development and Health
University of Southampton
Southampton, SO16 6YD, UK
E-mail:Ric hard.Oreffo@soton.ac.uk

DOI:10. 1002/adfm.201202710

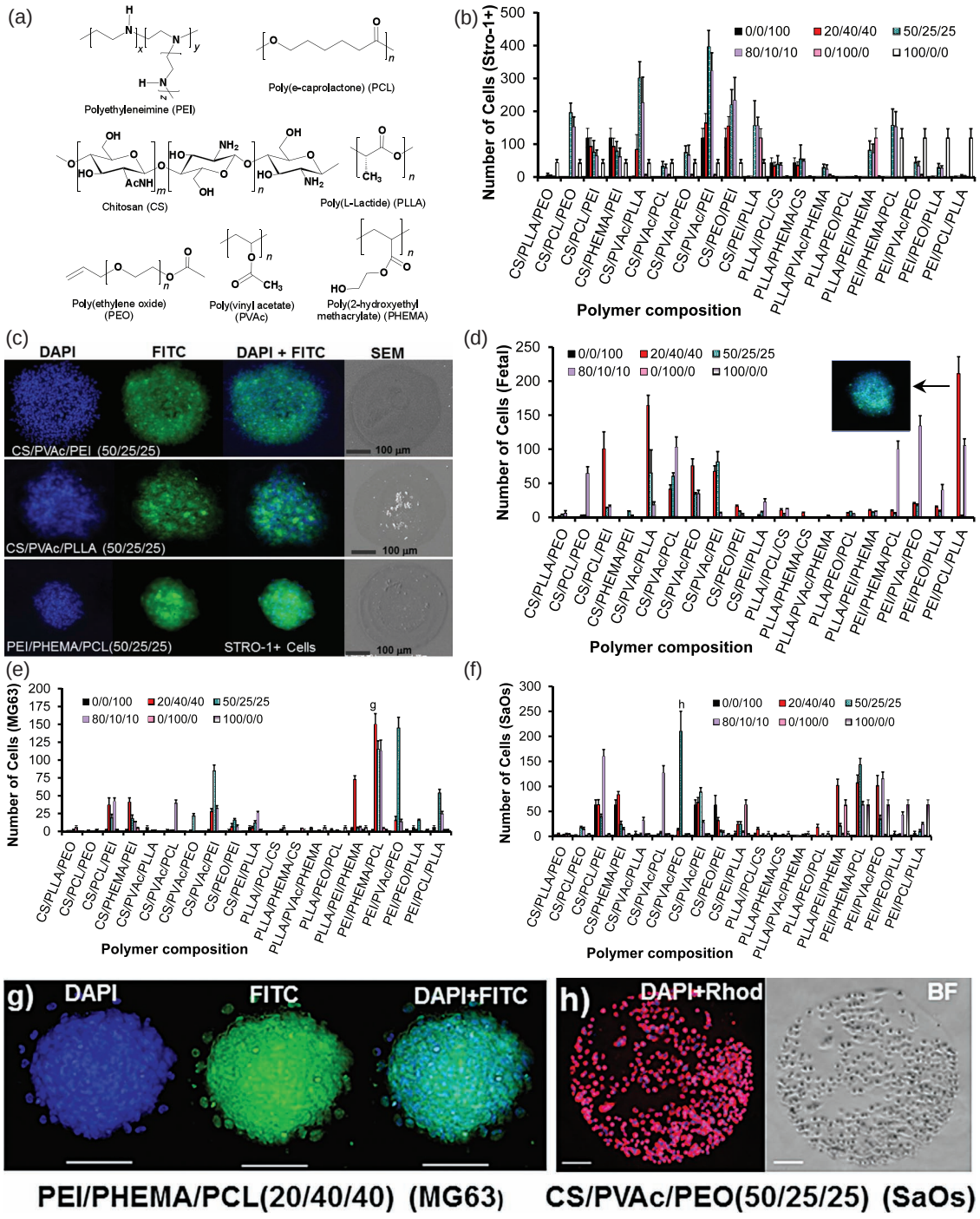

Figure 1. Identification of ternary polymer blends as potential scaffold materials for skeletal tissue bioengineering. a) Chemical structures of the polymers utilized in the generation of the ternary blend arrays. STRO-1+, fetal skeletal cells, MG63 (cytoplasm stained with the viability marker CellTracker Green or Red) and SaOs (with CellTracker Red) (cell nuclei stained with Hoechst-33342) were incubated on the ternary polymer blend microarray slides for 18 h. The bound cells were fixed, and the microarrays were scanned with a high-content microscope based scanner. b) Analysis of STRO-1+ cells binding to each polymer blend composition (n = 4). c) Examples of STRO-1+ binding affinities with DAPI, FITC and (DAPI+FITC) images on three selected ternary polymer blends: CS/PVAc/PEI (50/25/25), CS/PVAc/PLLA (50/25/25) and PEI/PHEMA/PCL (50/25/25), with corresponding SEM images (right). d) Assessment of fetal skeletal cellular attachment onto each polymer blend (n = 4). e–h) Binding affinity analysis of two human osteosarcoma cell lines, MG63 (e, g) and SaOs (f, h), on the ternary blend microarrays (n = 4), with representative examples of images of cell binding (g, h). g) DAPI, FITC and merged (DAPI+FITC) images of MG63 cells on the PEI/PHEMA/PCL (20/40/40) blend. h) Images of SaOs cells on the CS/PVAc/PEO (50/25/25) blend, with DAPI and Rhodamine (left image) and bright field (BF) (right image). Results (b, d, e, and f) are presented with ±SD. Scale bar = 100 µm (g) and 50 µm (h).

act as matrix materials to support the growth of the early osteoblast-like MG63 cell line, the mature osteoblast-like SaOs cell line, human bone marrow-derived STRO-1+ skeletal stem cells and human fetal femur-derived skeletal cells. Following these studies the most suitable polymers were generated *en masse* and assessed for skeletal tissue regeneration using a variety of *in vitro* and *in vivo* approaches.

2. Results and Discussion

2.1. Design, Fabrication, and Characterization of Ternary Polymer Blends

Ternary polymer blends were generated from commercially available polymers, of both natural and synthetic origins, and included chitosan (CS), poly(ε-caprolactone) (PCL), poly(L-lactide) (PLLA), poly(vinyl acetate) (PVAc), poly(2-hydroxyethyl methacrylate) (PHEMA), poly(ethylenimine) (PEI) and poly(ethylene oxide) (PEO). CS is a natural cationic polysaccharide, derived from chitin by deacetylation, and is known to be biocompatible[35] and has attracted significant attention in biomedical science and tissue engineering applications.[36–38] PLLA and PCL are biodegradable polymers,[39] which have been utilized extensively in biomedical device fabrication and drug delivery.[40,41] PHEMA has been used in a range of applications including intraocular (contact) lenses, soft-tissue replacement, and applications to prevent cellular adhesion and spreading.[42] PEI is a cationic polymer which has been utilized for gene delivery,[43] however clinical application has been limited by its cytotoxicity. PEO is extensively used in biotechnology[44] since this polymer prevents protein adsorption, while PVAc has established application in wound healing and controlled drug release.[45] However, all these materials have different properties, and for effective biomedical applications, further processing and/ or engineering of these materials is often required. In this study, a series of functional biomedical materials were generated via solution blending with each blend consisting of three polymers in different ratios contact printed onto a glass slide. The surface morphology of the blended compounds is critically important for its biological application and is dictated by the multi-phase behavior of the materials and these properties were examined by scanning electron microscopy (SEM) (see Figure 1c and Supporting Information Figure S1). Highly porous 3D architectural scaffolds (**Figure 2**) were fabricated by freeze drying, with solid-liquid phase separation taking place, to give multiple porous scaffolds after solvent removal.

2.2. Attachment and Growth of STRO-1+ Cells, Fetal Skeletal Stem Cells, and Osteosarcoma Cell Lines (MG63 and SaOs) on the Ternary Polymer Blends Arrays

Screening of the blend arrays[6] with STRO-1+ cells and fetal skeletal stem cells and two human osteosarcoma cell lines (MG63 and SaOs) revealed significant differences in cellular attachment and growth (see Figure 1b–h and Supporting Information Figure S2 and S3).

Thus blends of PEI/PHEMA/PCL (in all ratios) supported attachment of both MG63 and SaOs cells, as did blends of CS/PCL/PEI, CS/PHEMA/PEI and CS/PVAc/PEI, however SaOs cell binding affinity was noticeably higher than MG63 in all cases. For example, the blend of CS/PVAc/PEO (ratio 50/25/25) showed significantly higher SaOs cell (210 ± 40) attachment, compared to MG63 cells (22 ± 3). Some blends also showed binding selectivity, thus the blend CS/PVAc/PLLA (ratio 80/10/10) bound SaOs, but not MG63 cells.

Fetal skeletal cell binding (Figure 1d and Supporting Information Figure S2c,d) typically showed very similar binding profiles as STRO-1+ cells (for example see the blends CS/PVAc/PLLA and CS/PVAc/PEI in Figure 1), although displaying a far higher affinity.[6,26] Array analysis also revealed some distinct polymer blend specificity (see Figure 1b,d), for example PEI/PCL/PLLA (ratio of 20/40/40 and 80/10/10) demonstrated significant binding of fetal skeletal cells (Figure 1d), but weak or no binding of STRO-1+ cells (Figure 1b).

Several blends, such as CS/PLLA/PEO, PLLA/PEO/PCL and PEI/PCL/PLLA displayed few if any STRO-1+ cell binding, while fetal skeletal cells displayed similar results for CS/PLLA/PEO and PLLA/PEO/PCL blends.

Following microarray analysis, four blends displaying high STRO-1+ cell compatibility [CS/PVAc/PEI(50/25/25), CS/PVAc/PLLA(50/25/25), CS/PEI/PLLA(50/25/25) and PEI/PHEMA/PCL(50/25/25)] were selected for detailed 3D investigation of STRO-1+ cell growth and differentiation on these scaffolds.

2.3. 3D Scaffolds and In Vitro Assessments

2.3.1. Fabrication and Characterization of 3D Scaffolds

A series of 3D scaffolds with porous network architecture were generated, however only the polymer CS/PVAc/PLLA (50/25/25) formed a structurally robust 3D scaffold suitable for bone engineering (see details in Supporting Information Table S2–S5). The physical properties of the polymer scaffold play a critical role in bone formation.[46,47] Figure 2 shows the analysis of the porous network of CS/PVAc/PLLA (50/25/25), with SEM images captured (Figure 2b–f) from the cross-section (parallel to the diameter, Figure 2a) showing an interconnected networks with open-ended pores, sized between 5 and 10 μm. SEM images of the scaffold in vertical cross-section (Figure 2g) showed continuous porous channels (50–600 μm) that can be attributed to the direction of solvent evaporation. The channel walls (Figure 2f,h,i) also consisted of small pores with an average pore diameter of approximately 580 nm (arrows indicated in Figure 2f,h). Large interconnected pores have been reported as being necessary for tissue growth and vascularization in bone-graft applications, whist a minimum size of 100 μm was demonstrated by Ravaglioli.[48] Furthermore, pore sizes above 200 μm are essential for the osteoconductivity of the scaffold to allow bone tissue regeneration.[49,50]

Several reports[51–53] have also demonstrated that pores in the nanometer range can enhance cell adhesion and proliferation at the implant site, and have the potential to absorb proteins and growth factors.[51,52] The scaffold blend [CS/PVAc/PLLA(50/25/25)] (Figure 2) showed a combination of pores in the sub-micron range within a macro-porous framework, with

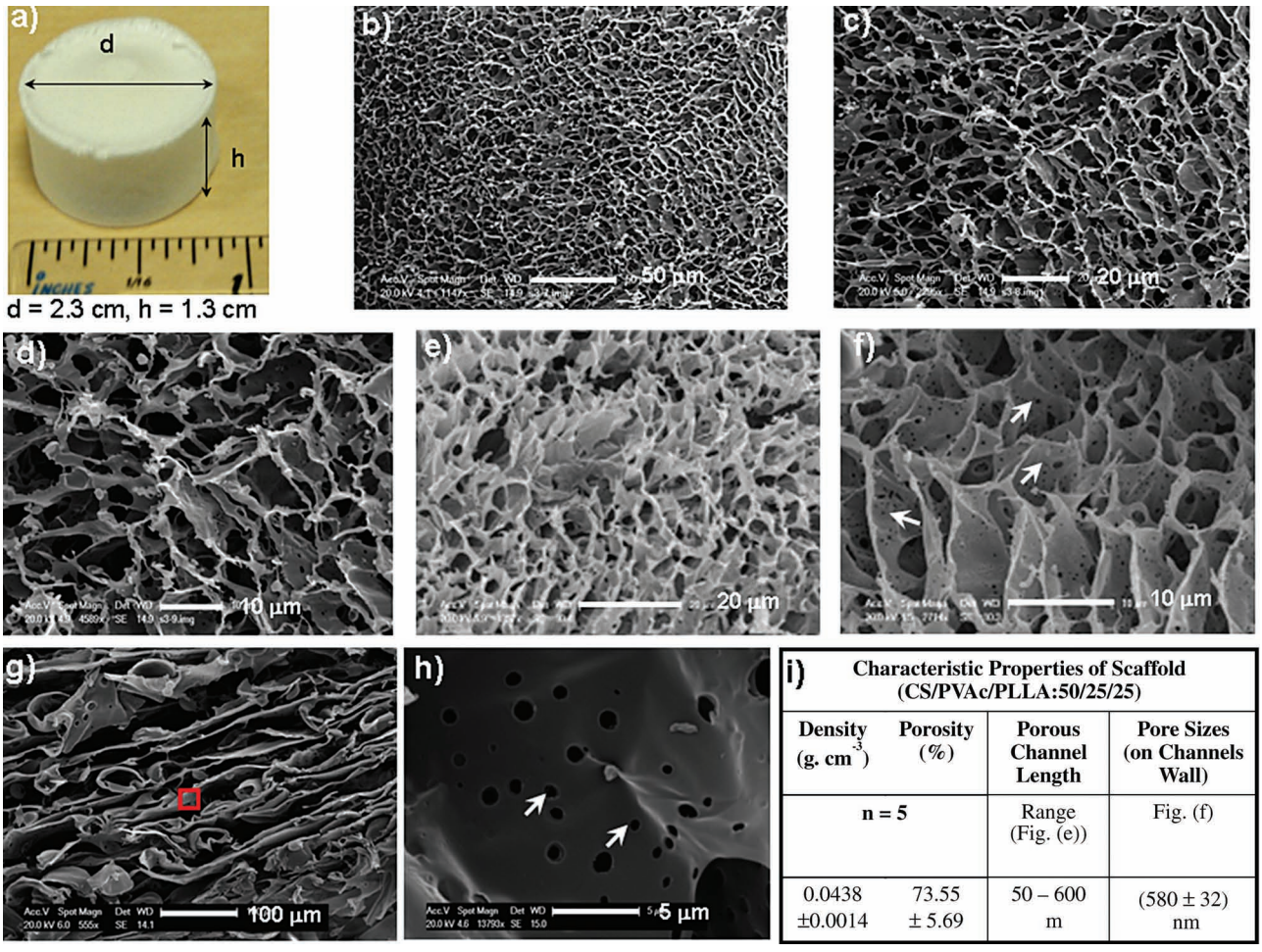

i) Characteristic Properties of Scaffold (CS/PVAc/PLLA:50/25/25)

Density (g. cm^{-3})	Porosity (%)	Porous Channel Length	Pore Sizes (on Channels Wall)
n = 5		Range (Fig. (e))	Fig. (f)
0.0438 ±0.0014	73.55 ± 5.69	50 – 600 m	(580 ± 32) nm

Figure 2. Fabrication of a scaffold generated from a blend of CS/PVAc/PLLA (50/25/25) and its physical characterization. a) Image of the 3D scaffold (diameter = 2.3 cm and height = 1.3 cm) prepared by freeze drying using a solvent-evaporation technique. b–f) SEM images of horizontal cross-sections of the scaffold with low (b); and higher magnifications; c-f) showing the porous network structure; g) SEM image of a vertical cross-section of the scaffold shows porous channel formation between 50–600 µm length, and each channel wall consists of a submicron pore structure; h) (highlighted in (g)), arrows indicate sub-micrometer pores (f, h). i) The physical properties of the scaffold (± SD) (n = 5).

an overall porosity of 74%, providing a structure very akin to that of trabecular bone.[51,53] The mechanical properties such as tensile strength (330 Pa), elongation at break (9.7%) and stiffness (0.83) of CS/PVAc/PLLA (50/25/25) blend were evaluated (supporting information Table S2) and indicated that this ternary blend had sufficient strength and stiffness for tissue engineering application.

2.3.2. In Vitro Biocompatibility, Growth, and Differentiation of STRO-1+ Cells on 3D Scaffolds

Detailed analysis of the structure and properties of ternary polymer blended scaffold [CS/PVAc/PLLA (50/25/25)] clearly revealed a similar architecture to natural trabecular bone (Figure 2). This scaffold was used to examine whether this blend enhanced STRO-1+ skeletal stem cell growth and differentiation, and therefore could be applied in bone tissue engineering.

3D scaffolds of CS/PVAc/PLLA (50/25/25) were found to function as excellent biomimetic scaffolds and promoted STRO-1+ cell attachment and growth over 28 days, in *in vitro* cultures (**Figure 3**). Prolific expression of alkaline phosphatase (ALP), an early marker of osteogenic differentiation,[54] was observed in the STRO-1+ progenitor cell population following a culture period of 28 days (Figure 3b,c). Quantitative analysis of ALP expression was performed by image analysis (Image J), and ALP expression was found to be 65% under osteogenic conditions, following 28 days of culture. Cell viability on the 3D biomimetic scaffold as assessed by CellTracker staining revealed excellent STRO-1+ cell viability after 28 days (Figure 3e,f) with the cells uniformly distributed as demonstrated by confocal microscopy (Figure 3e,f,h,i). Such effects were significantly enhanced under osteogenic culture conditions (see Figure 3a,d,g). Further evidence to support cells viability came from ethidium homodimer staining (to detect dead and/or dying cells) with no dead cells detected following culture on the 3D scaffold by confocal microscopy analysis, suggesting extremely high cell viability.

The CS/PVAc/PLLA scaffold also supported osteogenic differentiation of the STRO-1+ skeletal progenitors into mature

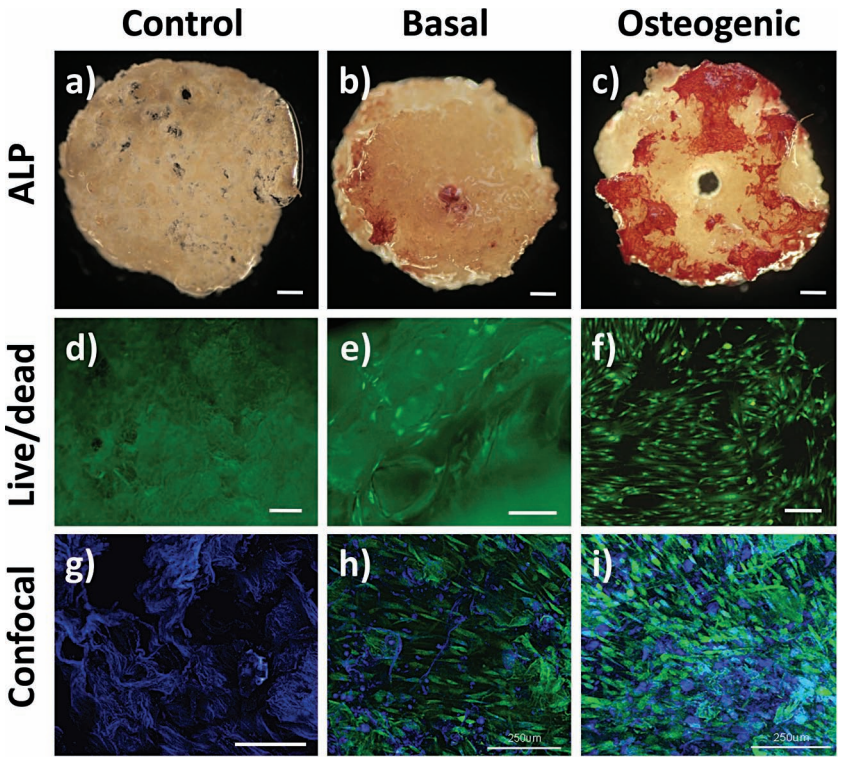

Figure 3. STRO-1+ cells were grown onto CS/PVAc/PLLA (50/25/25) scaffolds for 28 days, in two different (basal and osteogenic) culture conditions and compared to control samples containing no cells; a–c) Alkaline phosphatase (ALP) expression indicates early osteogenic differentiation; d–f) STRO-1+ cell proliferation was analyzed using viability staining (CellTracker Green), while no dead cells were observed with the nuclear stain ethidium homodimer (red). g–i) Confocal images of viable STRO-1+ cells labeled with CellTracker Green with the autofluorescence of the polymer matrix superimposed using the DAPI filter (blue). Scale bars: a–c) 500 µm, d–f) 200 µm, g–i) 250 µm.

osteoblasts under osteogenic culture conditions (culture media supplemented with human bone morphogenic protein (rhBMP-2), ascorbate and dexamethasone), as confirmed by immunocytochemical analysis of the expression of collagenous and non-collagenous bone matrix proteins:[54] Collagen Type I (**Figure 4**a,b), Osteopontin (Figure 4c,d), Bone Sialoprotein (BSP) (Figure 4e,f) and Osteonectin (Figure 4g,h) were all expressed by cells after 28 days culture. This was confirmed by the absence of staining on all negative controls (with and without cells), visualized using the same threshold values (Figure 4i,j). Thus, under osteogenic conditions under long term *in vitro* culture, the scaffolds composed of CS/PVAc/PLLA (50/25/25) facilitated the generation of a mature osteoblast population from the STRO-1+ skeletal stem cell population, indicating the suitability of this scaffold as a 3D matrix to assist skeletal stem cell regeneration including cellular attachment, growth, viability and osteogenic (early and mature) differentiation.

2.4. In Vivo Investigation for New Bone Formation in Segmental Defects

2.4.1. 3D Scaffold Implantation and Bone Regeneration Analysis

In order to investigate bone tissue regeneration strategies, a series of *in vivo* experiments were designed based on our previous data, utilizing an innovative load-bearing critical-sized murine femoral defect model.[55] Three series of *in vivo* experiments were conducted, each series consisting of four mice. The first series (control group) had a critical diaphyseal defect created within the femur, and was stabilized by intramedullary fixation, using a silicone disc as a control spacer. The same procedure was used to create a femoral defect for the second and third series. The CS/PVAc/PLLA (50/25/25) scaffolds were implanted into the femoral defect without STRO-1+ cells in the second series, whereas in the case of the third series STRO-1+ (5×10^6) cells were seeded onto each polymer [CS/PVAc/PLLA (50/25/25)] scaffold prior to implantation into the femoral defect.

To assess the positioning of the diaphyseal defect, intramedullary device and scaffold, and to visualize bone formation, an *in vivo* digital X-ray imaging technique was used over the four week study period. In addition 3D images of the entire femora were generated by micro-computed tomography (μCT) analysis following 28 days implantation to evaluate the extent of bone healing in femoral defects implanted with cell-seeded scaffolds, scaffolds alone, or spacers (**Figure 5**). No intra-operative or post-operative deaths occurred during the study period.

High resolution μCT scans of the defect regions at day 28 clearly demonstrated the formation of new bone in the defect regions implanted with the CS/PVAc/PLLA scaffold. New calcification was positioned appropriately in relation to the segmental defect site, with evidence of robust bone formation (Figure 5). Radiographic images of STRO-1+ cells seeded onto polymer scaffolds before implantation showed extensive new bone tissue formation at day 28, with calcified tissue filling the osteotomy site and in several cases extending well beyond this region. All samples in this series showed complete bone bridging within or around the osteotomy site. In all samples supplemented with STRO+ cells, there was also evidence of surrounding callus formation and in several specimens there was bone formation at ectopic sites not seen in either of the other groups. This ectopic bone formation correlated with the position of the scaffold and was interfaced to the new bone within the osteotomy site. Results demonstrated bone generation within the defect regions at day 28 was significant for both scaffold series (second and third) as compared to control samples. The difference was found to be less marked in bone regeneration between the second and third series of *in vivo* experiments.

To assess bone remodeling, we analyzed the indices of bone histomorphometry from the 3D μCT data (Figure 5b). An increasing trend was observed in bone volume (BV) (Figure 5bi) in the defect regions implanted with scaffold alone and scaffold with cells, although this increase was statistically insignificant

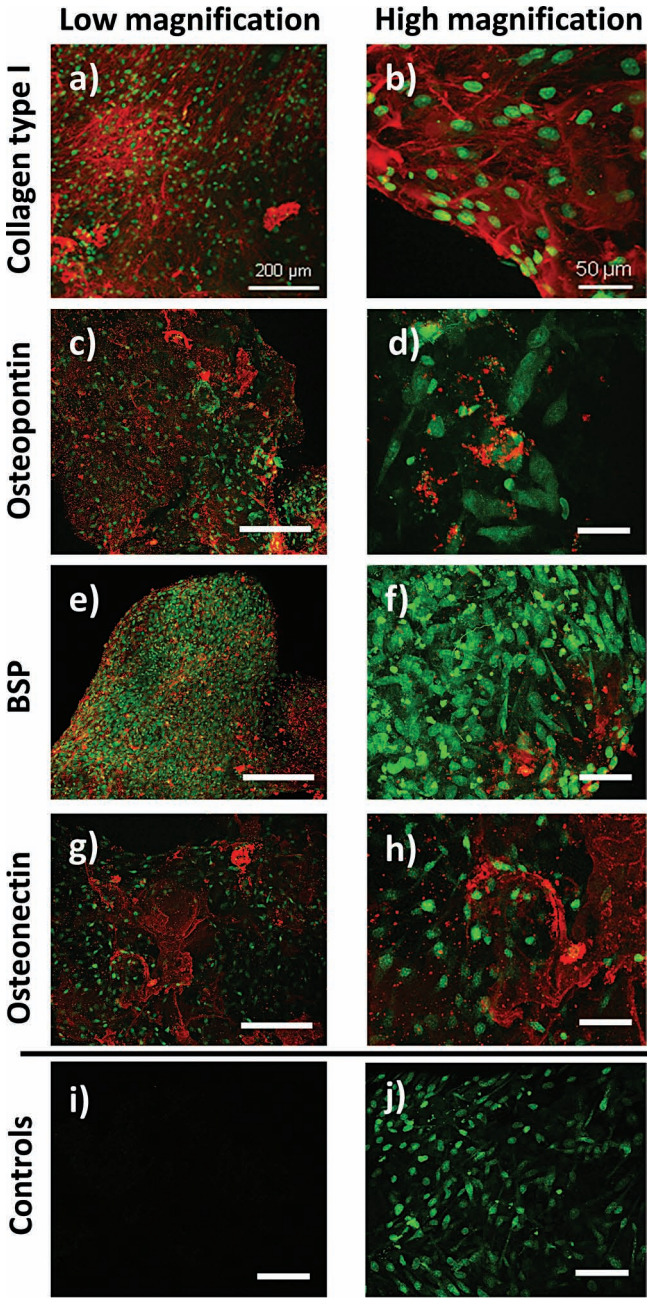

Figure 4. Immunostaining for osteogenic bone-matrix proteins of STRO-1+ cells cultured on the ternary polymer blend scaffold: CS/PVAc/PLLA (50/25/25). Cell nuclei are stained with DAPI (green) and each bone-matrix protein is stained by the Alexa 594 fluorochrome-conjugated secondary antibody (red). Confocal microscopic images show a,b) Collagen type I, c,d) osteopontin, e,f) bone sialoprotein (BSP), g,h) osteonectin, (i) negative control without cells, and (j) negative controls with cells.

with respect to the control implant. The trabecular bone volume: total volume ratio (BV/TV) in control samples was significant lower (3.9 ± 1.3) than either series where the defect regions were implanted with scaffold alone (increased by 2.3 fold (8.9 ± 2.3 **)) or scaffold with cells (increased by 2.6 fold (10.2 ± 1.6 **)), although insignificant differences were observed between the two test scaffold series (Figure 5b (ii)). Analysis of trabecular number (Tb No) demonstrated (Figure 5b (v)) an increase in bone trabecula within the defect regions, corresponding to the implanted cell-seeded scaffolds (4.2 ± 0.4 **), compared to scaffolds alone (3.5 ± 0.8 *), and such an increase was significantly higher for both groups when compared to the control (spacer) series (1.9 ± 0.6). In addition, a decrease in trabecular spacing (Tb Sp) which corresponds to the distance between adjacent trabecula was seen in the femoral defect region implanted with the cell-seeded scaffolds and scaffolds alone, as compared to the control (spacer) (Figure 5b (vi)). Furthermore, significantly lower bone surface to bone volume (BS/BV) ratios (Figure 5b (iii)) and a significantly higher trabecular thickness (Tb Th) (Figure 5b (iv)) were demonstrated for both scaffold implantation series in comparison to the control samples.

2.4.2. Histological Analysis of Defect Regions

For each specimen, transverse sections of the entire femur were constructed at low magnification to enable identification of regions of interest. Control samples typically showed negligible or no bone formation within or around the defect site. Following Alcian blue/Sirius red (A/S) staining, the cortical bone of the mouse femora were stained red with Sirius red, and the physeal zones that contain proteoglycans stained blue with Alcian blue, however there was universally negligible stain around the defect site (**Figure 6**a–c). CS/PVAc/PLLA blend scaffolds implanted alone exhibited significantly more cellular activity within and around the defect region (Figure 6d–i). A/S staining revealed the cut ends of the bone at the osteotomy sites closed over with new bone matrix, similar to the empty defect controls. In contrast, however, the site occupied by the blend scaffolds containing cells had significant cellular infiltration (seen particularly in Figure 6g–i). Fragmented remains of the polymer were visible on high power images, with new trabecula forming around these pieces (Figure 6e,f,i). These new trabecula formed at sites distant to the osteotomy (Figure 6h,i), although the whole process was well-defined within a 'pseudo-capsule', bounded by the femoral musculature. A high concentration of infiltrated cells (Figure 6g) was observed in an area directly between the two bone-ends within the defect region. A/S staining of the entire femoral sections containing either CS/PVAc/PLLA blend scaffolds or scaffold and implanted STRO-1+ cells revealed abundant osteoid formation with the development of morphologically normal trabecula and cellular infiltration (Figure 6j–n). This group of samples also showed a mature chondrocytic differentiation particularly at the intersection of the newly laid down matrix, with evidence of endochondral ossification ('watershed' area of Figure 6j–n).

Staining with Goldner's trichrome again confirmed trabecula within the metaphysis, containing multiple cells, however few cells were present within or around the defect, and no osteoid was laid down, evidenced by an absence of red staining (Figure 6a). Collagen type I immunohistochemistry stained positive in areas of existing cortical bone and also around the edges of the defect site, however there was limited collagen type I activity around the defect of the control samples (**Figure 7**a). Collagen type I immunostaining of scaffolds implanted with the

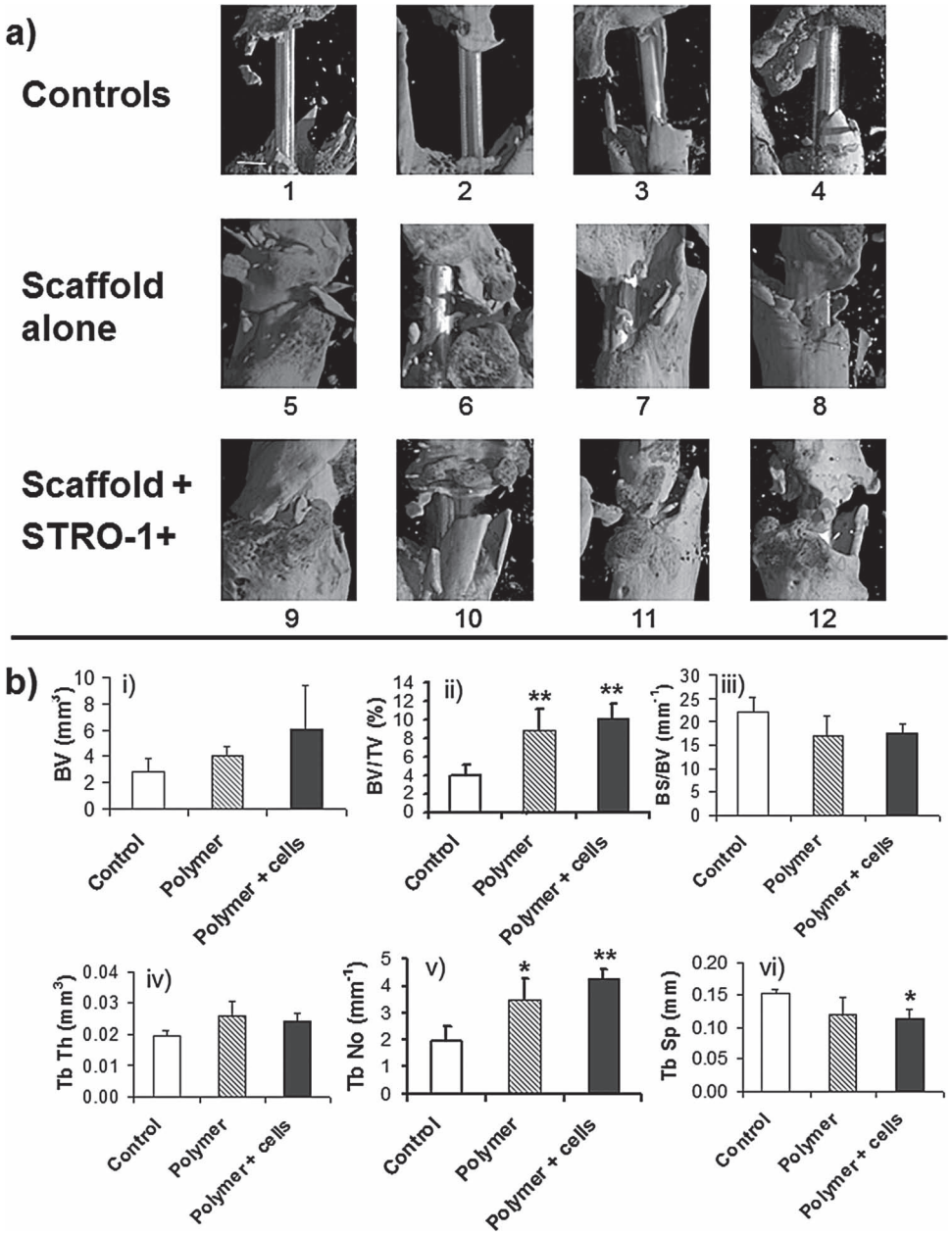

Figure 5. Quantitative μCT analysis for bone tissue regeneration of selected regions of interest within the osteotomy defect after 28 days. a) The intramedullary device is visible in these specimens, but was digitally subtracted prior to quantitative analysis of bone formation (scale bar = 1 mm). Enhanced bone formation is demonstrated in both scaffold groups (without and with STRO-1+ cells, respectively) when compared to the control group. b) Assessment of new bone regeneration in the defect regions in femora of mice at 28 days following implantation, using indices of bone volume (BV), bone volume/total volume (BV/TV), bone surface/bone volume (BS/BV), trabecular thickness (Tb Th), trabecular number (Tb No) and trabecular spacing (Tb Sp). Results are presented as mean ± SD, n = 4 per group, * = $p < 0.05$, ** = $P < 0.005$.

polymer blend alone revealed positive expression throughout the femoral cortex as seen previously, but staining was also observed within the defect region, and throughout those areas infiltrated with cells (Figure 7b–e). The expression of collagen type I was enhanced in the group implanted with polymer blend scaffolds (CS/PVAc/PLLA) and STRO-1+ cells, and such expression was seen throughout the trabecula of the newly-formed bone within the defect site (Figure 7f–i), similar to that of native bone.

Immunohistological analysis for von Willebrand's Factor (vWF) was performed for all three series of samples (**Figure 8**). Minimal staining for vWF was encountered around the defect sites of control samples (Figure 8a–c), although some staining of the cells within the medullary canal occurred, consistent with normal endothelial cell activity within this region. The vWF staining showed limited expression for blend scaffolds alone within the defect region (Figure 8d–g), however, the positive expression for vWF indicated cellular infiltration

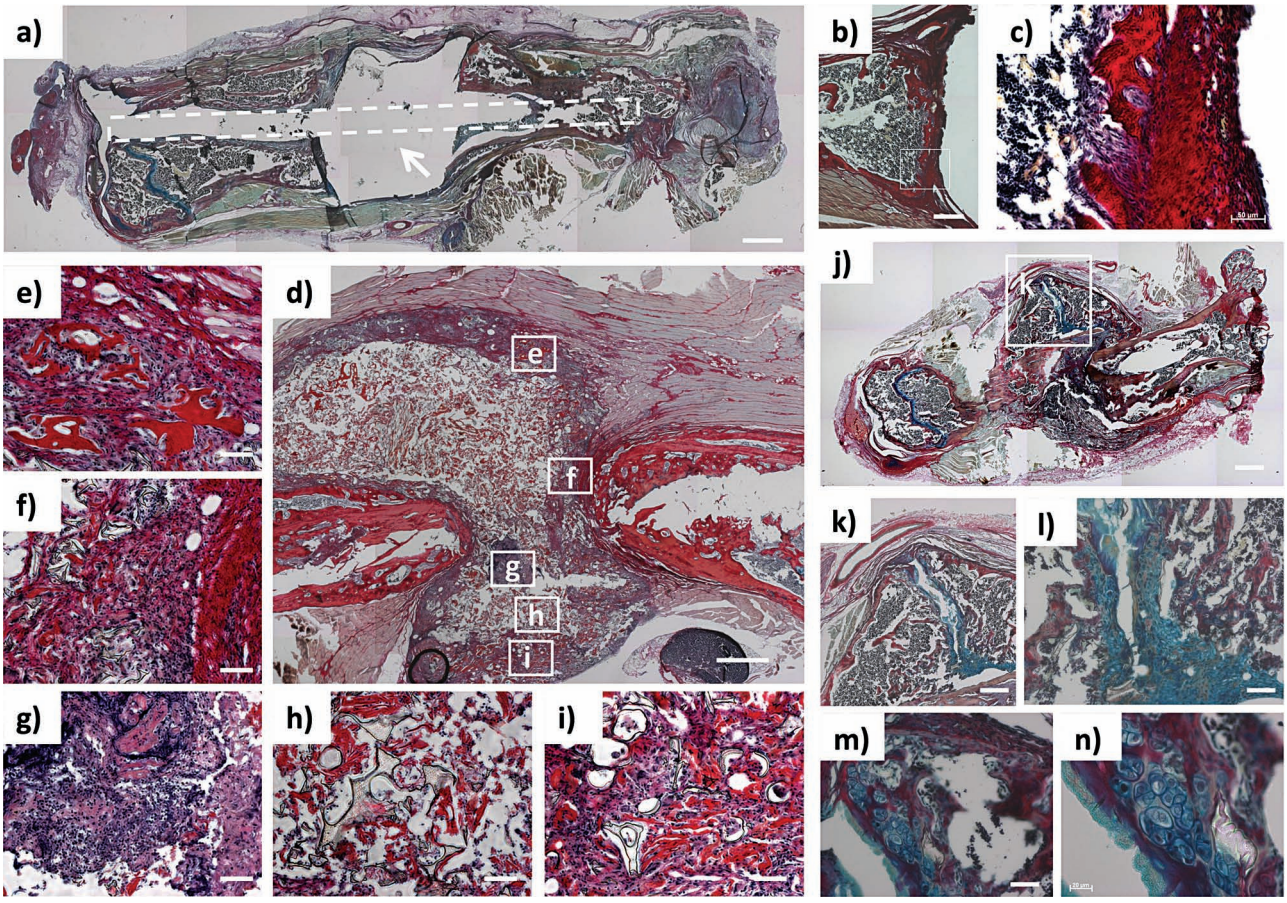

Figure 6. Histological analysis of the murine femoral segmental defect of three groups of samples stained with Alcian blue and Sirius red (A/S). a–c) Images of proximal femur and defect region of empty control samples. a) Whole femur, showing the empty control diaphyseal defect (arrow), and the intramedullary defect made by the nail (outline). b–c) High power images of a different control specimen demonstrate new collagen formation (red staining) around the edges of the defect, however this does not extend into the defect site. d–i) Femoral segmental defect treated with polymer group alone, stained with A/S. Note the significant cellular infiltration and new osteoid seen within a distinct 'pseudo-capsule' between the two bone ends. e) The cut end of the bone has sealed with new osteoid and significant trabecular bone formation is seen around this area. f) A peripheral area demonstrating fragmented remains of the translucent polymer scaffold surrounded closely by new osteoid (red) and cells (cell nuclei stained with Weigert's haematoxylin). g) A central region directly between the bone ends with significant cell infiltration and evidence of osteoid formation. h, i) Peripheral zones, both distant from the defect region showing abundant cells and bone formation, consistent with callus formation. j–n) Femoral segmental defect treated with polymer scaffolds seeded with STRO-1+ stem cells, stained with A/S. j) Demonstrating abundant new bone matrix within the osteotomy site and throughout the defect region. There is evidence of organized bone healing within a well-defined region around the osteotomy site, with mature trabecular formation and a 'watershed' area of chondrocytes suggesting a process of endochondral ossification. k) Well-defined trabecula are clearly seen with surrounding cellular infiltration. A distinct zone of chondrocytic differentiation is demonstrated at the interface between the two advancing bone matrix zones. An endothelial lined cyst is visible superficial to the regenerated bone area, which may represent a bursa, formed as a reaction to the intense bone-formation. l) 10× magnification image of the central regenerated area, demonstrating a distinct zone of chondrocytes. m) 2× magnification of the most superficial part of this zone; the chondrocytes are situated within the trabecula of newly-formed bone matrix. With increasing distance from this area, chondrocytes become progressively sparser, with increasing numbers of undifferentiated cells. n) 40× magnification of a region in (m). Clonal chondrocytic clusters are visible, suggestive of intense cellular activity and turnover in this region. Scale bars: a) 1 cm, b) 250 µm, c) 50 µm, d) 500 µm, e–i) 50 µm, j) 2 mm, k) 1 mm, l) 150 µm, m) 50 µm, n) 20 µm.

surrounded by tissue that stained positively (Figure 8d). The remaining fragments of polymer also demonstrated the brown oxidation product. This latter staining is unlikely to reflect true endothelial cell expression, but is readily distinguished from other regions of true expression, particularly in higher power images. vWF expression was also seen for the blend scaffolds implanted with STRO-1+ cells (Figure 8h–k). Results show vWF expression within the osteoid in the central defect area (Figure 8j), and several additional zones of vWF expression (Figure 8k).

3. Conclusions

This study has demonstrated the potential to generate functional biomaterials via the blending of three polymers to facilitate cell-attachment and differentiation suitable for skeletal regeneration strategies. Applying a high-throughput screening approach allowed the rapid identification of suitable blended materials for their ability to support skeletal progenitor cell growth and differentiation. Three candidate ternary polymeric blends were fabricated in sufficient quantities for macroscopic

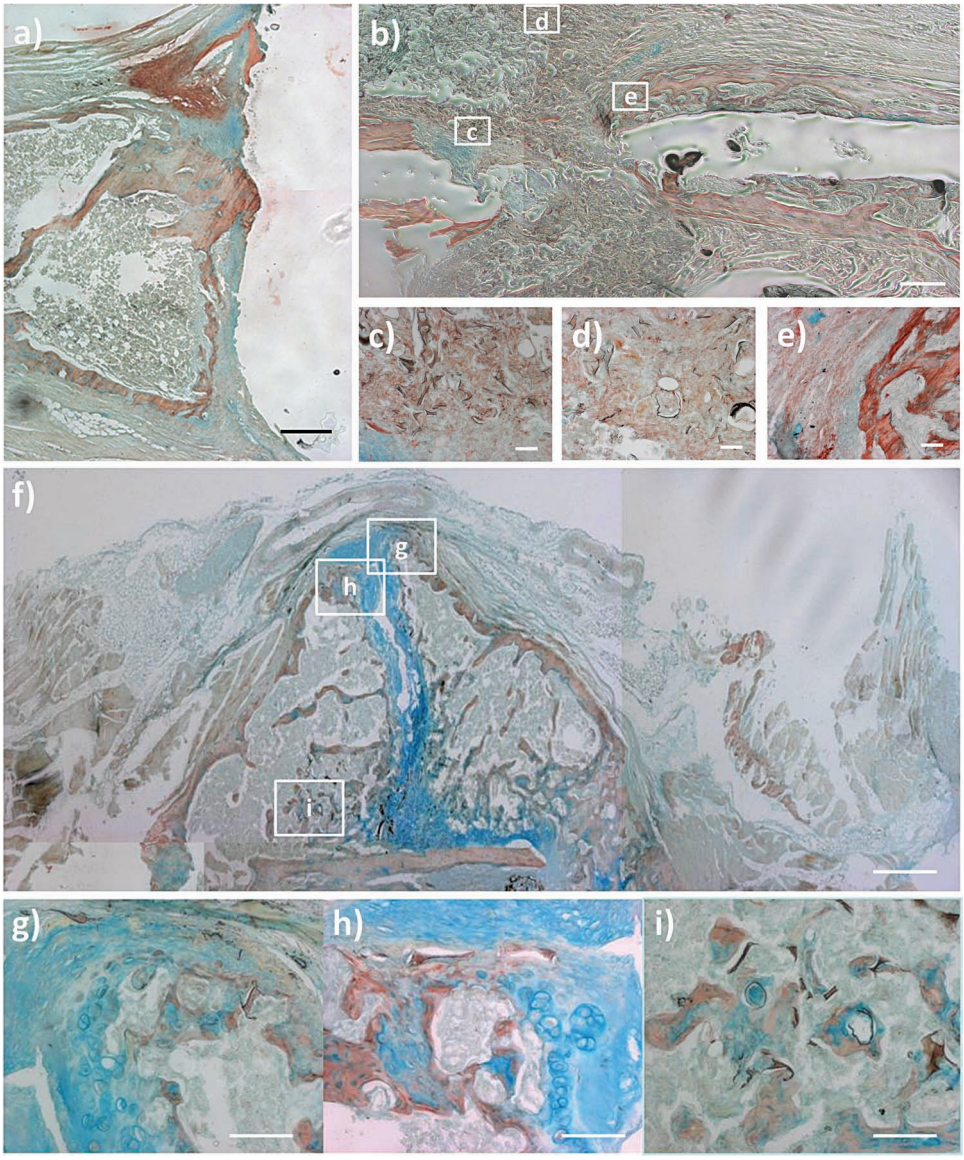

Figure 7. Analysis of collagen type I immunohistochemistry for three groups of samples. a) An empty defect controlled sample, b–e) polymer group alone showed increased expression throughout the defect region as compared to control samples, with localization to the new osteoid. f–i) Samples containing polymer scaffolds + STRO-1+ cells demonstrate expression throughout the newly-formed trabecula. g–i) Higher magnification images of regions of interest; g) Collagen type I expression is seen just behind the advancing zone of chondrocytes at the transition area; h) Expression is observed within some chondrocytes adjacent to the new bone; i) Fragments of polymer remain, these take up the brown stain, but are seen quite distinctly from the new bone formation on higher magnification sections. Scale bars: a) and b) 500 µm, c–e) 50 µm f) 1 mm, g–i) 200 µm.

analysis and then examined individually *in vitro* for their efficacy to support the generation of a differentiated osteoblast population of STRO-1+ skeletal stem cells. Critically, our high-throughput screening approach enabled the identification of the most efficacious blend (CS/PVAc/PLLA) for further detailed analysis as a robust 3D scaffold for skeletal tissue regeneration in immune-compromised mice, significantly reducing animal usage. The current data show that the polymeric ternary blend, CS/PVAc/PLLA was capable of enhancing skeletal regeneration, both *in vitro* and *in vivo*. Furthermore, we demonstrate that skeletal regeneration was enhanced by the incorporation of exogenous STRO-1+ cells with scaffolds as a true tissue engineering construct.

Radiographic analysis (including µCT reconstructions) demonstrated greater bone formation within the osteotomy site of the femora treated with the polymer blend when compared with controls and, critically, this was further enhanced by the addition of STRO-1+ cells to the scaffolds. Histological analysis strongly supported enhanced bone formation in this group, demonstrating additional cellular infiltration within the blend scaffold alone, which was further enhanced by the addition of STRO-1+ cells within the blend scaffold construct. Hydrolytic

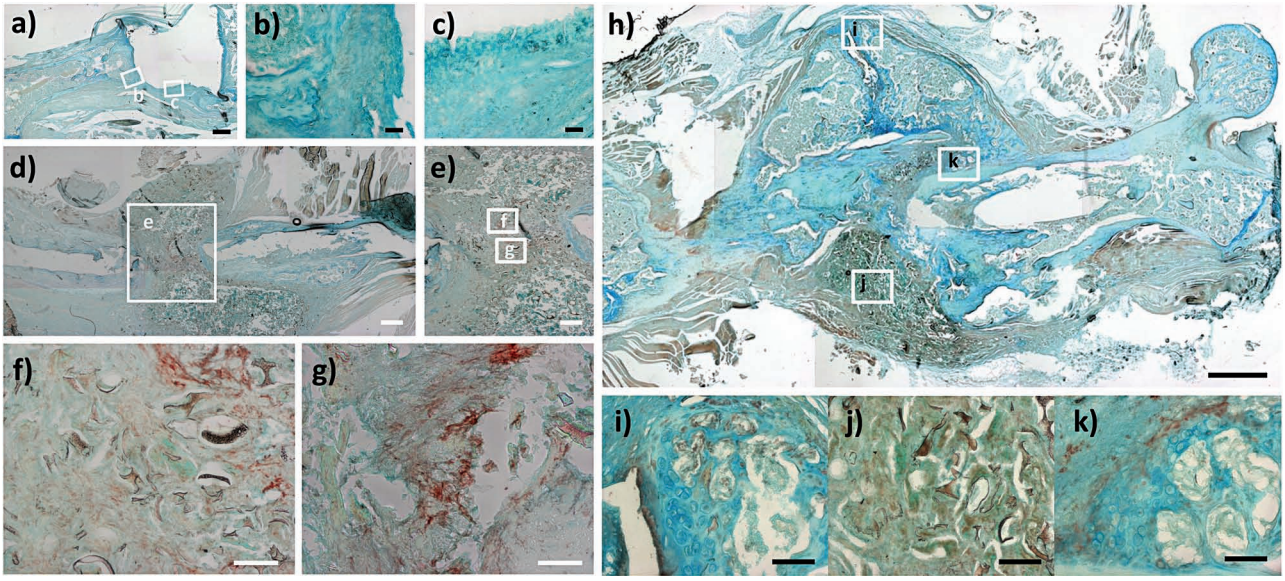

Figure 8. vWF immunohistochemistry of three groups of samples. a–c) An empty defect control sample. Low (a) and higher magnification areas (b, c) of a section stained for vWF show little staining around the defect site, although there was evidence of expression within the medullary canal. d–g) Polymer sample alone, confirming expression within the tissues surrounding the defect, and also to a limited degree within the defect region itself. Note the brown uptake of the remaining polymer fragments which is easily distinguished from true expression in the higher magnification images. h–k) Polymer scaffolds + STRO-1+ group sample, h) an entire femoral section, i) vWF expression is seen mainly around the undifferentiated cells behind the advancing area of chondrocytes, but there is also a discrete layer of expression within the space at the interface. j) vWF is expressed within the osteoid in the central defect area, it is seen distinctly from the staining of fragmented polymer. k) Several zones of vWF expression are seen, such as this layer demonstrated near the central area of the osteotomy defect. Scale bars: a) 500 µm, b–c) 50 µm, d) 1 mm, e) 200 µm, f–g) 50 µm, h) 2 mm, i)-k) 200 µm.

degradation of the polymer appeared to match new bone ingrowth, and new trabecula were seen in both cases with coincident, appropriate collagen type I expression.

Histological differences were encountered between the samples of polymer blend scaffolds alone and those containing STRO-1+ cells. The polymer scaffolds alone demonstrated the generation of woven bone within the osteotomy gap, while the latter samples demonstrated endochondral ossification, with a widespread callus reaction and mature chondrocyte development, prior to the formation of well-organized trabecula. Endothelial tissue infiltration into and around the osteotomy site (as demonstrated by positive vWF staining) was confirmed in both polymer groups, suggesting the presence of vascularization – a pivotal pre-requisite for osteogenesis.

In summary, we demonstrate the potential of translating high-throughput polymer chemical array strategies through *in vitro* analysis to identify functional ternary polymer blends for bone repair from microarray to *in vivo* preclinical evaluation. Current work on the translation of this technology to larger scale clinical models (ovine) are ongoing in our laboratories to validate the ternary blend biomaterials for functionality with respect to weight-bearing and remodeling capacity prior to clinical application.

4. Experimental Section

Materials: Chitosan (CS), polyethylenimine (PEI), agarose (Type 1-B), Poly(L-lactic acid) (PLLA) and Silane-Prep microscope slides were from Sigma-Aldrich (Gillingham, UK), Poly(ε-caprolactone) (PCL), Poly(ethylene oxide) (PEO), Poly(vinyl acetate) (PVAc) and Poly(2-hydroxymethyl methacrylate) (PHEMA) were from Scientific Polymer Products (Ontario, USA). Analytical grade chloroform, glacial acetic acid, N-methyl-2-pyrrolidinone (NMP) and Hoechst-33342 were from Thermo Fisher Scientific, UK.

Ternary Polymer Blend Preparation for Array Printing: CS was dissolved in 2% aqueous acetic acid to give a 1% w/v solution, which was filtered (20 µm). PEI and PHEMA were dissolved in NMP and PCL, PLLA, PEO and PVAc were dissolved in $CHCl_3$/NMP (1:1) to give 1% w/v solutions. These homopolymer solutions were blended into 57 ternary combinations (see supporting information Table S1). Each of these 19 ternary polymer blends were then fabricated in three different proportions (20:40:40, 50:25:25, 80:10:10) which were contact-printed onto agarose-coated (1.2 µm thick) Silane-Prep slides using a QArray mini printer (Genetix, New Milton, UK) with 16 aQu solid pins. The printing conditions comprised of 5 stamps per spot, 200 ms inking time and 10 ms stamping time, resulting in a typical spot size of 300–400 µm in diameter, with a distance of approximately 750 µm between adjacent spots. Multiple slides were printed with identical polymer microarrays to generate four replicates, and then the slides were dried for 24 h under vacuum at 40 °C.

Scanning Electron Microscopy: A scanning electron microscope (Philips XL30CPSEM) was used to investigate the surface morphology of the polymer microarrays and the polymer scaffolds. For microarray analysis, the glass slides containing the polymer arrays were attached to a specimen holder and coated with Au by sputtering, and the micrographs of arrays were captured at 10 kV in a secondary electron imaging mode. For scaffold analysis, the samples (0.5 cm × 0.5 cm × 0.5 cm) of different cross-sections were mounted onto the surface of the specimen holder and coated with Au, and images were taken at 15 kV.

STRO-1+ Skeletal Stem Cell Isolation and Culture: Bone marrow samples (n = 3) were collected from hematologically normal

osteoarthritic and osteoporotic individuals undergoing routine hip replacement surgery, with approval of the Southampton & South West Hampshire Local Research Ethics Committee (LREC194/99).[6,26] Skeletal stem cells (STRO-1+) from bone marrow were isolated by magnetically activated cell sorting (MACS) as described in the literature.[6,56,57] The isolated STRO-1+ skeletal stem cells were expanded by culturing them to confluence in monolayers in basal culture medium (α-MEM supplemented with 10% FCS).

Fetal Skeletal Cells: Femora from human fetuses (age: 8–11 weeks post-conception) were collected after the termination of pregnancies according to the guidelines issued by the Polkinghorne Report and with ethical approval from Southampton & South West Hampshire Local Research Ethics Committee. Cells were isolated from these predominantly cartilaginous femora[58] and cultured to confluence in monolayers in basal culture medium.

Protocol for Cell Culture on Microarrays: The ternary polymer blend microarrays were sterilized under UV irradiation for 30 min. STRO-1+ skeletal stem cells were isolated from 3 bone marrow samples, fetal skeletal cells were from 3 distinct fetal femora. The MG63 and SaOs cells were labeled with both CellTracker Green and CellTracker Red following manufacturer's instructions. Suspensions of the above mentioned cell populations in 1.5 mL basal media were pipetted onto the microarrays (10^6 cells/microarray slide, n = 3 microarray slides per cell type), so that the entire microarray surface was covered with a thin layer of cell suspension. The cells were incubated on the microarrays overnight at 37 °C, 5% CO_2 in humidified atmosphere. The following day, microarrays were thoroughly washed using PBS to remove any unbound/loosely-bound cells and the cells bound to the microarray spots were fixed using 4% paraformaldehyde in PBS. Nuclei of cells were stained using DAPI. Analysis was accomplished using an automated microscope equipped with the Pathfinder software (IMSTAR S.A., Paris, France). Cell binding to the polymer blends was ascertained by imaging individual polymer spots using a Zeiss Axiovert 200 inverted microscope.

3D Scaffold Fabrication and Characterization: The selected polymer blend scaffolds were fabricated using solutions of CS (2% w/v) in 2% (v/v) acetic acid and 98% deionized water, PLLA (10% (w/v), PVAc (10% w/v) in chloroform and PEI (20% w/v) in water, which were then thoroughly mixed using a vortex mixer for 15 min (typically volumes were approximately 20 mL). The blended solutions were frozen in liquid nitrogen and freeze dried (in a glass vial) while maintaining a temperature of –20 °C until no solvent remained, yielding scaffold cylinders (approximately 23 mm diameter × 40 mm height). All scaffolds were characterized using SEM along with image analysis for pore sizes. Despite modifications to the solvent evaporation technique, the blend of PEI/PHEMA/PCL(50/25/25) was not mechanically stable in a 3D configuration, so only blends CS/PVAc/PEI (50/25/25), CS/PEI/PLLA (50/25/25) and CS/PVAc/PLLA (50/25/25) underwent further analysis *in vitro*. Pieces of scaffold were cut using a razor blade to give the required sizes and shapes required for *in vitro* and *in vivo* investigations.

The porosity values of the scaffolds were measured by the liquid displacement method as described in published literature.[59] Briefly, a scaffold sample of weight W was immersed in a graduated cylinder containing a known volume (V_1) of ethanol. The sample was kept in the ethanol for 2 h under a constant mechanical vibration at 25 °C, and then a series of brief evacuation–repressurization cycles was conducted to force the ethanol into the pores of the scaffold. Cycling was continued until no air bubbles were observed emerging from the scaffold. The total volume of ethanol and the ethanol-impregnated scaffold then was recorded as V_2. The volume difference, ($V_2 - V_1$) was the volume of the polymer-blend skeleton of the scaffold. The ethanol-impregnated scaffold was removed from the cylinder and the residual ethanol volume recorded as V_3. The quantity ($V_1 - V_3$), the volume of the ethanol held in the scaffold, was determined as the void volume of the scaffold. Thus the total volume of the scaffold was: $V = (V_2 - V_1) + (V_1 - V_3) = V_2 - V_3$. The density of the scaffolds (ρ) was evaluated as, $\rho = W/(V_2 - V_3)$, and the porosity (ε) was obtained as, $\varepsilon = (V_1 - V_3)/(V_2 - V_3)$.

The porous structure of all scaffolds was evaluated using SEM (Philips XL30CPSEM), with the same sample preparation and image capturing techniques (as discussed in SEM section), approximately 100 pores of each scaffold were measured with Image J software for pore sizes.

In Vitro Cell Culture: Multiple discs (4 mm diameter × 1.5 mm height) were cut from the scaffold cylinders using sterile tissue biopsy punches (NHS Supply Chain, Alfreton, UK). Initially scaffolds were assessed by immersion in the standard solutions used for processing and analysis to ensure insolubility and maintenance of a robust structure following these processes. *In vitro* cell culture was performed for up to 28 days to validate the experimental technique, to confirm results of the microarray analysis of initial cell adherence and viability, and to ensure maintenance of appropriate scaffold structural properties following culture. Following sterilization overnight by exposure to UV irradiation, two discs of each polymer blend were mounted onto 21 gauge needles and seeded with 10^7 STRO-1+ cells in 2 mL of basal medium and gently agitated for 12 h. Subsequently, one disc of each polymer was incubated at 37 °C in 5% humidified atmosphere in either basal medium (supplemented with 10% FCS) or osteogenic medium (basal medium supplemented with 100 ng/mL rhBMP-2, 100 µM ascorbate-2-phosphate and 10 nM dexamethasone) for up to 28 days with medium changes every third day. 5 mL of medium was removed from each sample and pH was tested using a digital Bench pH meter (Hanna Instruments, Bedfordshire, UK) to detect potentially harmful acidic breakdown product from the scaffolds.

Immunohistochemical Analysis: Each fixed disc was cut into quarters and the resulting samples were combined and split into five groups for immunohistochemical analysis of osteogenic expression with five discrete markers. 1% BSA in PBS was used as the blocking buffer for 5 min, before application of the appropriate primary antibody, diluted in 1% BSA in PBS: anti-type I collagen (LF-67, rabbit polyclonal, 1:300 dilution) and anti-osteonectin (LF-8, rabbit polyclonal, 1:100 dilution) were provided by Dr. L Fisher; anti-bone sialoprotein (rabbit polyclonal 1:100 dilution) was provided by Dr. J Sodek, and anti-osteopontin (rabbit polyclonal, 1:100 dilution) were from GeneTex Inc. (Irvine, California, USA). Samples were incubated overnight at 4 °C prior to rinsing in running water and immersion for 5 min in each of three wash buffers containing: Trizma wash (12.1 g 50 mM tris[hydroxymethyl] aminomethane (Trizma base, Sigma), 1 mL 0.05% polyoxyethylene-sorbitan monolaurate (Tween 20, Sigma), 2l H_2O) and (a) high salt (46.7 g NaCl), (b) low salt (17.4 g NaCl) and (c) double concentration Trizma wash (0.1 M), adjusted to pH 8.5. Following complete removal of the final wash buffer, 100 µL of appropriate Alexa 594 fluorochrome-conjugated secondary antibody (monoclonal (anti-mouse) diluted 1:50, polyclonal (anti-rabbit) diluted 1:30 in 1% BSA in PBS) was applied at room temperature for one hour, before rinsing and incubating with 300 nM diamidino-2-phenylindole (DAPI, 1:100 dilution with PBS) nuclear counterstain (Invitrogen) for 5 min. Samples were stored in dark conditions at 4 °C before visualization with confocal microscopy, using a Leica SP5 laser scanning confocal microscope and software (Leica Microsystems, Wetzlar, Germany). Negative controls (i.e., omission of the primary antibodies) were included in all immunostaining protocols.

In Vivo Studies of the Mouse Segmental Femur Defect Model: A standard mouse femoral bone defect model was used, with a 5 mm femoral diaphyseal segmental osteotomy for a 28 day study period. This part of the study was carried out in accordance with the protocol described previously.[55,60] In brief, four MF-1 nu/nu immunodeficient mice in three study groups underwent the procedure: For the control group, a critical diaphyseal defect was made in the femur, and stabilized with intramedullary fixation, using a silicone disc as a control spacer. The second group underwent the same procedure, except with interposition of the polymer scaffold alone within the defect. The third group received the polymer scaffold which had been seeded with 5×10^6 STRO+ cells. Correct needle placement was confirmed by Faxitron specimen X-ray imaging (MX-20, Qados Ltd, Sandhurst, UK). Following death, the entire right femur of each mouse was disarticulated for analysis. Plain radiographic analysis was performed by Faxitron imaging prior to fixation of each sample in periodate-lysine-paraformaldehyde (PLP) fixative for 48 h. Quantitative 3D analysis was performed using the X-TEK benchtop

160Xi CT scanner for micro-computed tomography (X-TEK Systems Ltd, Tring, UK), equipped with a Hamamatsu C7943 X-ray flat panel sensor (Hamamatsu Photonics, Welwyn Garden City, UK). Samples were scanned using a molybdenum target at 100 kV, 70 µA, with an exposure time of 2134 ms and 1x digital gain. Following successful data acquisition and initial image reconstruction of each entire femur with a 15 µm voxel resolution, the femora were decalcified in Tris-EDTA (0.1 M tris(hydroxymethyl) aminomethane-5% ethylenediaminetetraacetic acid) at pH 7.3, for 4 weeks.

In Vivo CT Image Analysis: Following image reconstruction, a constant region of interest with dimensions 5 mm × 5 mm × length of original defect, was assigned within each femur with reference to the Faxitron images acquired at day 0 and 28. The reconstructed images were visualized and analyzed using Studio Max 1.2.1 software (Volume Graphics GmbH, Heidelberg, Germany). Manual thresholds were selected to exclude soft tissue and scaffold, and the metal intramedullary needles were digitally subtracted to quantify bone volume, bone surface/bone volume, bone volume/total volume, trabecular number, trabecular thickness and trabecular spacing. GraphPad Prism software was used for statistical analysis. Differences between groups were determined by one-way ANOVA with a post hoc Tukey test and were considered to be significantly different if $p < 0.05$.

In Vivo Histological and Immunohistochemical Staining: Following decalcification, samples were dehydrated through graded ethanol concentrations, prepared with histoclear and embedded in low-melting point paraffin wax. Each sample was cut into twenty semi-sequential 6 µm sections before mounting onto glass microscope slides. Histochemical and immunohistochemical staining was performed for Weigert's hematoxylin/Alcian blue/Sirius red (A/S), Goldner's trichrome, Collagen type I and vWF respectively following de-waxing and hydration of each section, using standard protocols. Visualization of immunohistochemical product was achieved using the avidin/biotin method with peroxidise and 3-amino-9-ethylcarbazole (AEC). Negative control samples were included in each staining run, which yielded no evidence of staining.

Supporting Information

Supporting Information is available from the Wiley Online Library or from the author.

Acknowledgements

F.K. and J.O.S. contributed equally to this work. We acknowledge research funding from the Biotechnology and Biological Sciences Research Council, UK (Grant references: BB/FoF/245, BB/D01283X/1 and BB/DO13682). The authors gratefully acknowledge Dr. S Lanham for acquisition of computed tomography data, Dr. D Johnson for assistance with confocal microscopy, Miss E Ralph and Mrs C Roberts who undertook some of the histological protocols.

Received: September 18, 2012
Revised: November 15, 2012
Published online: January 25, 2013

[1] J. K. Park, J.-H. Shim, K. S. Kang, J. Yeom, H. S. Jung, J. Y. Kim, K. H. Lee, T.-H. Kim, S.-Y. Kim, D.-W. Cho, S. K. Hahn, *Adv. Funct. Mater.* **2011**, *21*, 2906.
[2] T. G. Kim, H. Shin, D. W. Lim, *Adv. Funct. Mater.* **2012**, *22*, 2446.
[3] M. D. Schofer, A. Veltum, C. Theisen, F. Chen, S. Agarwal, S. Fuchs-Winkelmann, J. R. J. Paletta, *J. Mater. Sci.: Mater. Med.* **2011**, *22*, 1753.
[4] M. D. Schofer, P. P. Roessler, J. Schaefer, C. Theisen, S. Schlimme, J. T. Heverhagen, M. Voelker, R. Dersch, S. Agarwal, S. Fuchs-Winkelmann, J. R. J. Paletta, *PLoS ONE* **2011**, *6*, 1.
[5] E. Tayton, M. Purcell, A. Aarvold, J. O. Smith, S. Kalra, A. Briscoe, K. Shakesheff, S. M. Howdle, D. G. Dunlop, R. O. C. Oreffo, *Acta Biomater.* **2012**, *8*, 1918.
[6] F. Khan, R. S. Tare, J. M. Kanczler, R. O. C Oreffo, M. Bradley, *Biomaterials* **2010**, *31*, 2216.
[7] a) C. Medine, F. Khan, S. Pernagallo, R. Zhang, O. Tura, M. Bradley, D. Hay, in *Biomaterials and Stem Cells in Regenerative Medicine* (Eds: M. Ramalingam, S. Ramakrishna, S. Best), CRC Press, **2012**, Ch. 1, pp 1-29; b) F. Khan, S. R. Ahmad, in *Biomaterials and Stem Cells in Regenerative Medicine* (Eds: M. Ramalingam, S. Ramakrishna, S. Best), CRC Press, **2012**, Ch. 5, pp 101–122.
[8] Y. Tanaka, H. Yamaoka, S. Nishizawa, S. Nagata, T. Ogasawara, Y. Asawa, Y. Fujihara, T. Takato, K. Hoshi, *Biomaterials* **2010**, *31*, 4506.
[9] D. Puppi, F. Chiellini, A. M. Piras, E. Chiellini, *Prog. Polym. Sci.* **2010**, *35*, 403.
[10] N. Mohan, P. D. Nair, *Tissue Eng., Part A.* **2010**, *16*, 373.
[11] A. T. Hillel, S. Unterman, Z. Nahas, B. Reid, J. M. Coburn, J. Axelman, J. J. Chae, Q. Guo, R. Trow, A. Thomas, Z. Hou, S. Lichtsteiner, D. Sutton, C. Matheson, P. Walker, N. David, S. Mori, J. M. Taube, J. H. Elisseeff, *Sci. Transl. Med.* **2011**, *3*, 1.
[12] L. Ma, C. Gao, Z. Mao, J. Zhou, J. Shen, X. Hu, C. Han, *Biomaterials* **2003**, *24*, 4833.
[13] P. Kuppan, K. S. Vasanthan, D. Sundaramurthi, U. M. Krishnan, S. Sethuraman, *Biomacromolecules* **2011**, *12*, 3156.
[14] Y. Yang, T. Xia, W. Zhi, L. Wei, J. Weng, C. Zhang, X. Li, *Biomaterials* **2011**, *32*, 4243.
[15] L. L. Y. Chiu, R. K. Iyer, L. A. Reis, S. S. Nunes, M. Radisic, *Front. Biosci.* **2012**, *17*, 1533.
[16] J. O. Smith, A. Aarvold, E. R. Tayton, D. G. Dunlop, R. O. C. Oreffo, *Tissue Eng., Part B* **2011**, *17*, 307.
[17] M. Mastrogiacomo, S. Scaglione, R. Martinetti, L. Dolcini, F. Beltrame, R. Cancedda, R. Quarto, *Biomaterials* **2006**, *27*, 3230.
[18] H. Ma, J. Hu, P. X. Ma, *Adv. Funct. Mater.* **2010**, *20*, 2833.
[19] L. Moroni, R. Schotel, D. Hamann, J. R. de Wijn, Cs A. van Blitterswijk, *Adv. Funct. Mater.* **2008**, *18*, 53.
[20] M. Deng, S. G. Kumbar, L. S. Nair, A. L. Weikel, H. R. Allcock, C. T. Laurencin, *Adv. Funct. Mater.* **2011**, *21*, 2641.
[21] C. T. Laurencin, A. M. A. Ambrosio, M. D. Borden, J. A. Cooper, *Ann. Rev. Biomed. Eng.* **1999**, *1*, 19.
[22] S. Weiner, W. Traub, *FASEB J.* **1992**, *6*, 879.
[23] G. Marotti, *Calcif. Tissue Int.* **1993**, *53*, S47.
[24] K. F. Leong, C. M. Cheah, C. K. Chua, *Biomaterials* **2003**, *24*, 2363.
[25] R. O. C. Oreffo, C. Cooper, C Mason, M. Clements, *Stem. Cell. Rev.* **2005**, *1*, 169.
[26] R. S. Tare, F. Khan, G. Tourniaire, S. M. Morgan, M. Bradley, R. O. C. Oreffo, *Biomaterials* **2009**, *30*, 1045.
[27] A. Liberski, R. Zhang, M. Bradley, *Chem. Comm.* **2009**, *48*, 7509.
[28] R. Zhang, A. Liberski, R. Sanchez-Martin, M. Bradley, *Biomaterials* **2009**, *30*, 6193.
[29] R. Zhang, A. Liberski, F. Khan, J. J. Diaz-Mochon, M. Bradley, *Chem. Comm*, **2008**, *11*, 1317.
[30] F. Khan, R. S. Tare, R. O. C. Oreffo, M. Bradley, *Angew. Chem. Int. Ed.* **2009**, *48*, 978.
[31] Y. Yang, D. Bolikal, M. L. Becker, J. Kohn, D. N. Zeiger, C. G. Simon Jr., *Adv. Mater.* **2008**, *20*, 2037.
[32] Q. Tran-Cong-Miyata, S. Nishigami, T. Ito, S. Komatsu, T. Norisuye, *Nat. Mater.* **2004**, *3*, 448.
[33] C. G. Simon Jr., N. Eidelman, S. B. Kennedy, A. Sehgal, C. A. Khatri, N. R. Washburn, *Biomaterials* **2005**, *26*, 6906.
[34] M. Bradley, F. Khan, R. O. C. Oreffo, R. S. Tare, Patent WO 2010023463 A2, **2010**.
[35] M. Rinaudo, *Prog. Polym. Sci.* **2006**, *31*, 603.

[36] S. Jana, S. J. Florczyk, M. Leung, M. Zhang, *J. Mater. Chem.* **2012**, *22*, 6291.
[37] T.-L. Yang, *Int. J. Mol. Sci.* **2011**, *12*, 1936.
[38] R. A. A. Muzzarelli, *Carbohyd. Polym.* **2009**, *76*, 167.
[39] K. Fukushima, Y. Kimura, *Polym. Int.* **2006**, *55*, 626.
[40] C. G. Simon Jr., N. Eidelman, S. B. Kennedy, A. Sehgal, C. A. Khatri, N. R. Washburn, *Biomaterials* **2005**, *26*, 6906.
[41] A. G. A. Coombes, S. C. Rizzi, M. Williamson, J. E. Barralet, S. Downes, W. A. Wallace, *Biomaterials* **2004**, *25*, 315.
[42] L. W. Norton, H. E. Koschwanez, N. A. Wisniewski, B. Klitzman, W. M. Reichert, *J. Biomed. Mater. Res., Part A* **2007**, *81A*, 858.
[43] S. C. De Smedt, J. Demeester, W. E. Hennink, *Pharm. Res.* **2000**, *17*, 113.
[44] C. V. Bonduelle, W. M. Lau, E. R. Gillies, *ACS Appl. Mater. Interfaces* **2011**, *3*, 1740.
[45] M. Jannesari, J. Varshosaz, M. M. M. Zamani, *Int. J. Nanomed.* **2011**, *6*, 993.
[46] V. Karageorgiou, D. Kaplan, *Biomaterials* **2005**, *26*, 5474.
[47] D. W. Hutmacher, *Biomaterials* **2000**, *21*, 2529
[48] A. Ravaglioli, A. Krajewski, *Bioceramics: Materials, Properties, Applications*. Chapman & Hall, London **1992**.
[49] T. T. Ajaal, R. W. Smith, *J. Mater. Process. Technol.* **2009**, *209*, 1521.
[50] E. Pamula, E. Filova, L. Bacakova, V. Lisa, D. Adamczyk, *J. Biomed. Mater. Res.* **2009**, *89A*, 432.
[51] A. Tampieri, F. Celloti, S. Sprio, A. Delcogliano, S. Franzese, *Biomaterials* **2001**, *22*, 1365.
[52] I. D. Xynos, A. J. Edgar, L. D. K. Buttery, L. L. Hench, J. M. Polak, *J. Biomed. Mater. Res.* **2001**, *55*, 151.
[53] D. R. Carter, W. C. Hayes, *J. Bone Jt. Surg. Am.* **1977**, *59*, 954.
[54] J. B. Lian, G. S. Stein, *Iowa Orthop. J.* **1995**, *15*, 118.
[55] J. M. Kanczler, P. J. Ginty, J. J. A. Barry, N. M. P. Clarke, S. M. Howdle, K. M. Shakesheff, R. O. C. Oreffo, *Biomaterials* **2008**, *29*, 1892.
[56] K. Stewart, S. Walsh, J. Screen, C. M. Jefferiss, J. Chainey, G. R. Jordan, J. N. Beresford, *J. Bone Miner. Res.* **1999**, *14*, 1345.
[57] D. Howard, K. Partridge, X. Yang, N. M. P. Clarke, Y. Okubo, K. Bessho, S. M. Howdle, K. M. Shakesheff, R. O. C. Oreffo, *Biochem. Biophys. Res. Commun.* **2002**, *299*, 208.
[58] S. H. Mirmalek-Sani, R. S. Tare, S. M. Morgan, H. I. Roach, D. I. Wilson, N. A. Hanley, R. O. C. Oreffo, *Stem Cells* **2006**, *24*, 1042.
[59] P. Zhang, Z. Hong, T. Yu, X. Chen, X. Jing, *Biomaterials* **2009**, *30*, 58.
[60] J. Kanczler, P. Ginty, L. White, N. Clarke, S. Howdle, K. Shakesheff, R. O. C. Oreffo, *Biomaterials* **2010**, *31*, 1241.